ISSN 1674-1056
http://cpb.iphy.ac.cn
http://iopscience.iop.org/cpb
中国物理 B
Chinese Physics
中国物理 Chinese Physics B

Equivalent magnetic dipole method used to design gradient coil for unilateral magnetic resonance imaging

Zheng Xu(徐征), Xiang Li(李想), Pan Guo(郭盼), Jia-Min Wu(吴嘉敏)
Citation: Chin. Phys. B . 2018, 27(5): 058702. **doi:** 10.1088/1674-1056/27/5/058702

Journal homepage: http://cpb.iphy.ac.cn; http://iopscience.iop.org/cpb

What follows is a list of articles you may be interested in

Nonlinear profile order for three-dimensional hybrid radial acquisition applied to self-gated free-breathing cardiac cine MRI

Yanchun Zhu(朱艳春), Pascal Spincemaille, Jing Liu(刘静), Shuo Li(李硕), Thanh D Nguyen, Martin R Prince, Yaoqin Xie(谢耀钦), Yi Wang(王乙)
Chin. Phys. B . 2017, 26(1): 018701. **doi:** 10.1088/1674-1056/26/1/018701

Accuracy and effectiveness of self-gating signals in free-breathing three-dimensional cardiac cine magnetic resonance imaging

Shuo Li(李硕), Lei Wang(王磊), Yan-Chun Zhu(朱艳春), Jie Yang(杨洁), Yao-Qin Xie(谢耀钦), Nan Fu(付楠), Yi Wang(王乙), Song Gao(高嵩)
Chin. Phys. B . 2016, 25(12): 128703. **doi:** 10.1088/1674-1056/25/12/128703

Linear-fitting-based similarity coefficient map for tissue dissimilarity analysis in T_2^*-w magnetic resonance imaging

Yu Shao-De, Wu Shi-Bin, Wang Hao-Yu, Wei Xin-Hua, Chen Xin, Pan Wan-Long, Hu Jiani, Xie Yao-Qin
Chin. Phys. B . 2015, 24(12): 128711. **doi:** 10.1088/1674-1056/24/12/128711

Flexible reduced field of view magnetic resonance imaging based on single-shot spatiotemporally encoded technique

Li Jing, Cai Cong-Bo, Chen Lin, Chen Ying, Qu Xiao-Bo, Cai Shu-Hui
Chin. Phys. B . 2015, 24(10): 108703. **doi:** 10.1088/1674-1056/24/10/108703

Multi-objective optimization of gradient coil for benchtop magnetic resonance imaging system with high-resolution

Wang Long-Qing, Wang Wei-Min
Chin. Phys. B . 2014, 23(2): 028703. **doi:** 10.1088/1674-1056/23/2/028703

Equivalent magnetic dipole method used to design gradient coil for unilateral magnetic resonance imaging*

Zheng Xu(徐征)[1,†], Xiang Li(李想)[1], Pan Guo(郭盼)[2,‡], and Jia-Min Wu(吴嘉敏)[1]

[1] State Key Laboratory of Power Transmission Equipment & System Security and New Technology, Chongqing University, Chongqing 400044, China

[2] School of Physics and Electronic Engineering, Chongqing Normal University, Chongqing 401331, China

(Received 15 December 2017; revised manuscript received 1 February 2018; published online 26 April 2018)

The conventional magnetic resonance imaging (MRI) equipment cannot measure large volume samples nondestructively in the engineering site for its heavy weight and closed structure. In order to realize the mobile MRI, this study focuses on the design of gradient coil of unilateral magnet. The unilateral MRI system is used to image the local area above the magnet. The current density distribution of the gradient coil cannot be used as a series of superconducting nuclear magnetic resonance gradient coils, because the region of interest (ROI) and the wiring area of the unilateral magnet are both cylindrical side arc surfaces. Therefore, the equivalent magnetic dipole method is used to design the gradient coil, and the algorithm is improved for the special case of the wiring area and the ROI, so the X and Y gradient coils are designed. Finally, a flexible printed circuit board (PCB) is used to fabricate the gradient coil, and the magnetic field distribution of the ROI is measured by a Gauss meter, and the measured results match with the simulation results. The gradient linearities of x and y coils are 2.82% and 3.56%, respectively, less than 5% of the commercial gradient coil requirement.

Keywords: unilateral MRI, equivalent magnetic dipole method, gradient coil, current density distribution

PACS: 87.61.–c, 84.32.Hh, 02.30.Zz **DOI:** 10.1088/1674-1056/27/5/058702

1. Introduction

Conventional magnetic resonance imaging (MRI) must work in highly homogeneous field,[1,2] but the volume and weight of the equipment restrict its applications, especially for huge object. For conventional closed magnet structures, the sample must be placed inside the magnet. However, the unilateral magnet provides a new direction of application for MRI.

Unilateral magnetic resonance imaging (UMRI) is a new type of nuclear magnetic resonance (NMR) measurement method. We use the characteristics of unilateral magnets to build a system to realize magnetic resonance imaging (MRI), which is called UMRI. Compared with conventional closed MRI, the UMRI can be easily moved for its open structure, small size, and the sample can be nondestructively tested from the surface above sample, obviously UMRI has a good prospect.[3,4] In recent years, the research on imaging systems based on UMRI equipment has also made some progress.[5–7] Blümich presented a two-dimensional (2D) phase-encoding imaging method to realize 2D imaging with a unilateral NMR probe.

The gradient coils play an irreplaceable role in MRI, which should be specially designed for unilateral magnet. At the same time, since the unilateral magnet has a static gradient field perpendicular to the surface of the magnet (the z-axis direction as shown in Fig. 1), we only need to design x and y gradient coils to realize a three-dimensional (3D) gradient.

The design of the gradient coil is an inverse problem of the electromagnetic field. The design method can be divided into regular separation winding method and distributed winding method.[8,9] The distributed winding method does not predetermine the shape of the coil, but rather calculates the desired current density distribution by a predetermined magnetic field distribution within the region of interest (ROI), and then use conductive copper plates or distributed winding to simulate the current density distribution, in order to determine the specific shape and size of the coil winding. This method is also easy to determine inductors, energy consumption and self-shielding constraints and other conditions. The design method includes stream function method,[10,11] target field method,[12,13] harmonic coefficient method,[14] and equivalent magnetic dipole method.[15,16] Owing to different magnet structures, the gradient coil design method is slightly different. At present, some design methods are applied to the design of coils in Halbach magnets,[17,18] which has some similarities to the unilateral magnet gradient coil design. However, in this paper the design of gradient coils for unilateral magnets is still lacking. We adopt the equivalent magnetic dipole method to design gradient coils, focusing on the characteristics of a unilateral magnet, and whose ROI and wiring area are both cylin-

*Project supported by the National Natural Science Foundation of China (Grant Nos. 51677008, 51377182, 51707028, and 11647098), the Fundamental Research Funds of the Central Universities, China (Grant No. 106112017CDJQJ158834), and the State Key Development Program for Basic Research of China (Grant No. 2014CB541602).

†Corresponding author. E-mail: xuzheng@cqu.edu.cn

‡Corresponding author. E-mail: guopan@cqnu.edu.cn

© 2018 Chinese Physical Society and IOP Publishing Ltd

drical side arc surfaces.

2. Unilateral MRI magnet structure

In this study, a unilateral MRI magnet was designed for mobile UMRI. The main magnetic field is parallel to the upper surface of the magnet. The default direction is the X direction as shown in Fig. 1. The magnetic field distribution in the ROI is shown in Fig. 2, and has a natural gradient in the direction of the vertical main magnetic field (Z direction). Therefore, the three-direction gradient magnetic field can be realized only by designing the gradient coils in the X and Y direction. Unilateral NMR sensor is shown in Fig. 3. The magnetic field strength in the center of the arc is 188.56 mT, corresponding to an NMR frequency of 8.02 MHz. The angle of ROI is 90°, the length of ROI is 60 mm, and the magnetic field uniformity in the ROI range is 1.5%. With passive shimming and active shimming, we make the magnetic field uniformity in the ROI reach 500 ppm below. The gradient of the center of the arc along the Z axis is 0.754 T/m.

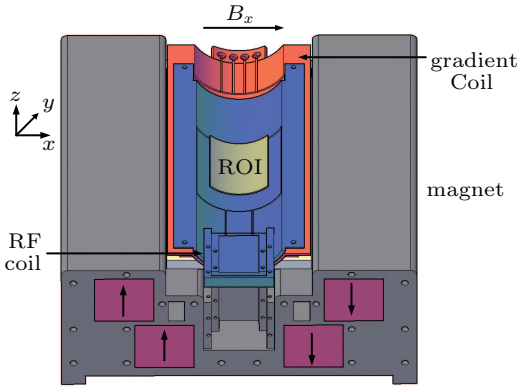


Fig. 1. (color online) Unilateral magnet structure diagram.



Fig. 2. (color online) Magnetic field distribution in the region of interest of the unilateral magnetic field.

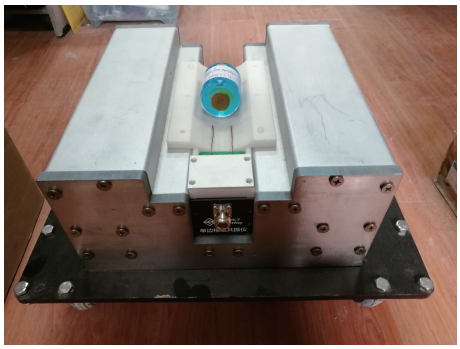


Fig. 3. (color online) Unilateral magnet sensor physical map.

3. Theory and method

In this paper, the wiring area of the gradient coil is a cylindrical side arc surface, and it can be divided into q units, each unit is a tiny cylindrical piece with thickness h, length a, and arc length a, as shown in Fig. 4. We assume that there is only one base current loop (or magnetic dipole) in each unit cylindrical piece. If each unit cylindrical pieces are small enough, the current paths formed by these base currents can be equivalent to the actual current distribution (the current flowing through each loop is I_n, the current flowing through the entire cylinder surface is I).

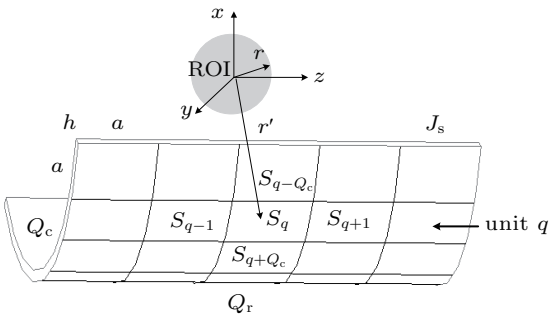


Fig. 4. Split cylindrical surface schematic diagram.

3.1. Stream function

According to the law of current continuity, important preconditions for current densities can be obtained as

$$\nabla \cdot \boldsymbol{J}_s(\boldsymbol{r}') = 0. \tag{1}$$

Therefore, we can define a hypothetical scalar stream function $S(\boldsymbol{r}')$ to represent the current density distribution

$$\boldsymbol{J}_s(\boldsymbol{r}') = \nabla \times S(\boldsymbol{r}') \cdot \boldsymbol{n}(\boldsymbol{r}'). \tag{2}$$

The stream function defines the function with the continuous direction changing in a limited area. Therefore, the stream function is suitable for the current distribution problem discussed in this paper. The stream function is used to describe the current density distribution of the base current in each split cylindrical surface, wherein the contour distribution of the stream function can represent the actual current routing, and the difference in stream function between the adjacent contour lines is the actual current value

$$I = \frac{S_{\max} - S_{\min}}{N}, \tag{3}$$

where $S_{\min}$ refers to the minimum value of the stream function, $S_{\max}$ represents the maximum value on the plane, N is the number of contour lines, and I is the current in each winding line.

3.2. Equivalent magnetization

We can solve the value of the stream function $S(\boldsymbol{r}')$ to obtain the winding structure, so we hope to establish the relationship between the stream function $S(\boldsymbol{r}')$ and the magnetic field $\boldsymbol{B}$ in the ROI. In this paper, we use an intermediate quantity (equivalent magnetization $\boldsymbol{M}(\boldsymbol{r}')$) to connect the stream function $S(\boldsymbol{r}')$ and the target magnetic field $\boldsymbol{B}$. Assuming that the magnetization of a single dipole is $\boldsymbol{M}(\boldsymbol{r}')$, and that the equivalent magnetizing current flows through each of the split cylindrical surfaces, the equivalent current density of the dipole can be obtained by the theory of electromagnetic field as follows:

$$\boldsymbol{J}_{\mathrm{s}}(\boldsymbol{r}') \approx \nabla' \times \boldsymbol{M}(\boldsymbol{r}')h. \tag{4}$$

Therefore, substituting Eq. (2) into Eq. (4), we can obtain the relationship between the equivalent magnetization and the stream function as follows:

$$\boldsymbol{M}(\boldsymbol{r}') \approx \frac{S(\boldsymbol{r}') \cdot \boldsymbol{n}(\boldsymbol{r}')}{h}. \tag{5}$$

3.3. Magnetic field in ROI

In Fig. 4, when the unit length a is sufficiently small, the value of the stream function in the unit cylinder q can be approximated by a constant S_q, and the area of the unit can be approximated as a^2. Let $\boldsymbol{n}_q$ denote the outer normal direction of unit q and assume that the cylinder surface is divided into Q_{c} columns along the circumference and Q_{r} rows along the axial z axis, and we will have totally $Q = Q_{\mathrm{c}}Q_{\mathrm{r}}$ units. The q is sorted according to the rows one by one as shown in Fig. 4. The difference between the numbers of the two adjacent cells in the left and right is 1, and the difference between the numbers of the two adjacent cells in the upper and lower is Q_{c}. These units of $q = 1 \sim Q_{\mathrm{c}}$ and $Q - Q_{\mathrm{r}} \sim Q$ are the upper and lower boundaries of the cylinder, respectively.

If $a \ll |\boldsymbol{r} - \boldsymbol{r}'|$, then a single magnetic dipole produces an equivalent magnetic moment

$$\boldsymbol{m}_q = \boldsymbol{M}a^2h = a^2S_q\boldsymbol{n}_q, \tag{6}$$

where S_q is the q-th magnetic dipole stream function value.

According to Eq. (2), the solution current distribution can be obtained by solving the value S_q of the stream function S on each dipole base coil. Equivalent magnetic dipole moment $\boldsymbol{m}$ is generated by the magnetic field expressed in the following formula:[17]

$$\begin{aligned}\boldsymbol{B} &= \frac{\mu_0}{4\pi}(\boldsymbol{m}\cdot\nabla)\nabla\frac{1}{r} = \frac{\mu_0}{4\pi}\nabla\left(\boldsymbol{m}\cdot\nabla\frac{1}{r}\right)\\ &= -\frac{\mu_0}{4\pi}\nabla\left(\boldsymbol{m}\cdot\frac{\boldsymbol{r}}{|r|^3}\right).\end{aligned} \tag{7}$$

Therefore, the relationship between the target magnetic field $\boldsymbol{B}$ and the magnetic dipole moment is obtained, then substituting Eqs. (5) and (6) into Eq. (7), the magnetic field value at this point (x, y, z) in the ROI is composed of the values of magnetic dipoles Q, which are generated by the source point x-direction magnetic field expression

$$B_x(x,y,z) = \frac{\mu_0 a^2}{4\pi}\sum_{q=1}^{Q} c_{x,q}S_q, \tag{8}$$

where

$$\begin{aligned}c_{x,q} &= R^{-5}[2(x-x_q)^2n_x - (y-y_q)^2n_x - (z-z_q)^2n_x + \cdots\\ &\quad 3(x-x_q)(y-y_q)n_y + 3(x-x_q)(z-z_q)n_z].\end{aligned} \tag{9}$$

In Eq. (9), n_x, n_y, and n_z denote the normal vectors outside the unit of cylinder, namely the components of $\boldsymbol{n}_q$ along the x, y, and z direction. Therefore, the relationship between target magnetic field $\boldsymbol{B}$ and stream function S_q is obtained. Since the target field is known, the coil structure can be obtained by solving S_q.

3.4. Optimizing strategy

If the design of the coil only makes the magnetic field in the ROI meet the target magnetic field, the structure of the gradient coil may be not smooth, which will increase the resistance of the coil and make the local temperature too high. Hence, the energy loss needs to be optimized. The energy consumption expression produced by all magnetic dipole elements can be written as

$$P = \sum_{q=1}^{Q}\left[(S_{q+1} - S_q)^2 + (S_{q+Q_{\mathrm{c}}} - S_q)^2\right]. \tag{10}$$

The optimal mathematical model is constructed as follows:

$$\begin{aligned}&\min: f = \sum_{q=1}^{Q}[(S_{q+1} - S_q)^2 + (S_{q+Q_{\mathrm{c}}} - S_q)^2],\\ &\mathrm{st}\quad B_x - B_{\mathrm{target}} = 0.\end{aligned} \tag{11}$$

The constraints in Eq. (11) are difficult to satisfy, making it difficult to solve the initial solution of the optimization problem, which leads to the interruption of the solution. Therefore, the penalty function can be constructed to transform the constraint problem into an unconstrained optimization problem, and then use the unconstrained optimization method to solve the problem. The coil constraint as a penalty function, is multiplied by the penalty parameter λ added to the optimization function f, because the penalty function is close to 0, and a large value of λ is required to make the penalty operation meaningful. The ROI is divided into N subregions, each corresponding to a field point. Then the optimal objective function is constructed as follows:

$$\min: F = \sum_{q=1}^{Q}[(S_{q+1} - S_q)^2 + (S_{q+Q_{\mathrm{c}}} - S_q)^2]$$

$$+\lambda \sum_{n=1}^{N} (B_x - B^{\text{target}})^2. \tag{12}$$

The latter item on the right-hand side in Eq. (12) is the square sum of the difference between the calculated magnetic field B_x and the target magnetic field B_{target} in the ROI, where B_x is calculated from Eq. (8). The target magnetic field is changed according to the design requirements, for example, for the x gradient coil, $B_{\text{target}} = G_x x$, for the y gradient coil, $B_{\text{target}} = G_y y$. The optimization problem of type (12) can be solved by the lsqnonlin toolbox of MATLAB software. Lsqnonlin library function uses the least square method for solving the nonlinear function in the following form:

$$\min_x \|f(x)\|_2^2 = \min_x (f_1(x)^2 + f_2(x)^2 + \cdots + f_n(x)^2), \tag{13}$$

where x is a vector or matrix and $f(x)$ is a function of the returned vector or matrix value. Equation (12) can be transformed to the least square form

$$\min : F = \sum_{n=1}^{N} \left(\sqrt{\sum_{q=1}^{Q} [(S_{q+1} - S_q)^2 + (S_{q+Q_c} - S_q)^2] + \lambda (B_x - B^{\text{target}})^2} \right)^2. \tag{14}$$

After obtaining the optimal value of the stream function S_q, the coil structure can be obtained by drawing the contour of the stream function. In addition, the optimal value of the penalty parameter λ needs to be determined. This requires the gradient linearity δ to be used as an optimization indicator, which is expressed as

$$\delta = \frac{\Delta B}{B_{\text{target}}} \times 100\%. \tag{15}$$

When δ is calculated, the magnetic field B is the B_x value calculated from Eq. (7), and B_{target} is the ideal magnetic field set above. The optimization steps are as follows.

(i) Set the initial value of λ to be $\lambda = 10^{10}$.

(ii) Obtain the optimal solution S_q from Eq. (13).

(iii) Calculate the B_x value by substituting S_q into Eq. (7) to further calculate the gradient linearity degree δ value.

(iv) Set the optimal exit conditions for $\delta < \varepsilon$, where ε is the gradient linearity requirement. When exit conditions are met, the loop ends. The current value λ is used as the optimal penalty parameter, or $\lambda_{k+1} = a\lambda_k$, where a is usually set to be $10^{[i]}$. Then repeat steps (ii)–(iv).

4. Results

4.1. Simulation results

According to the actual magnet structure and simulation parameter optimization, the wiring area of the gradient coil in this paper is a 200-mm-length cylindrical side arc surface. Its radius is 45 mm, and its central angle is 120°. Wiring area is divided into 50 subareas equally in the X, Y direction, and is divided into a total of 2500 units, each unit can be approximated as a square, split unit side length a total. The ROI is a cylindrical surface with a radius of 35 mm central angle of 90°, length of 60 mm. We divide the cylindrical surface into 100 area elements, each corresponding to a target field point. Using the above analysis we can carry out the calculation to obtain the X and Y gradient coil.

When designing the gradient coil, at $\lambda = 10^{10}$, we set the parameter $\varepsilon = 3\%$ to exit from the loop to obtain X, Y gradient coil, and the structure of the gradient coil can be obtained as shown in Figs. 5(a) and 6(a). Then we use the Biot–Savart law to verify the magnetic field of the gradient coil simulated. The magnetic field distributions in the ROI of the X and Y gradient coil when the current of 1 A is provided are shown in Figs. 5(b) and 6(b), respectively.

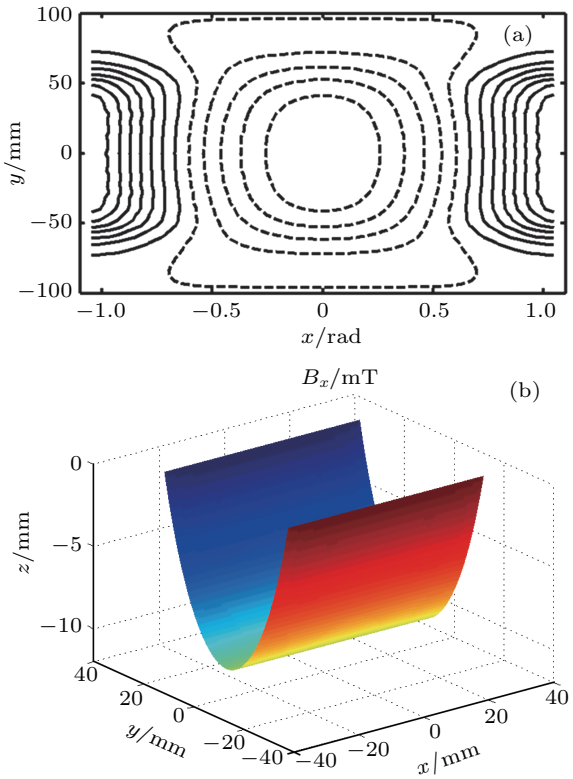


Fig. 5. (color online) X direction gradient coil, showing (a) gradient coil contour and (b) magnetic field distribution of the ROI of the XoY plane.

As the conventional coil resistance is too large, more serious heat is produced, we use the anti-coil structure to reduce the coil resistance. The final structure is shown in Fig. 7, the red area above is the ROI, and the blue and dark red areas be-

low are the X and Y gradient coil.

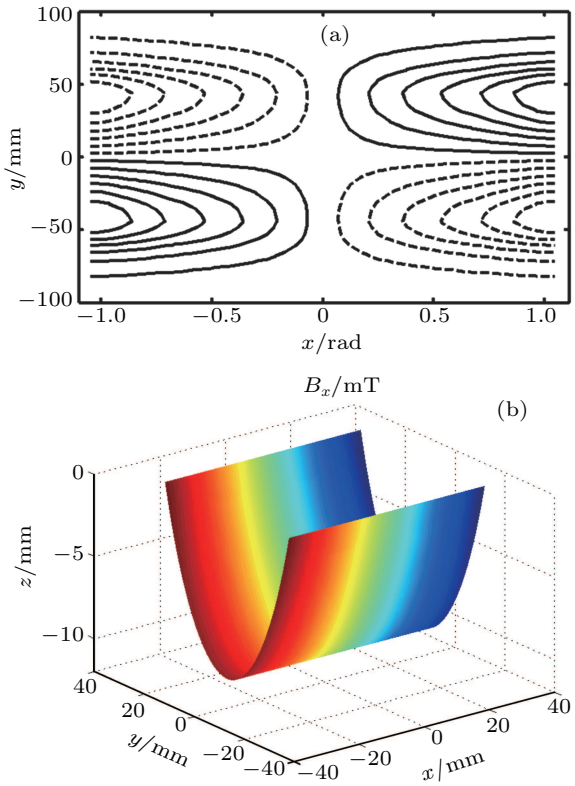


Fig. 6. (color online) Y direction gradient coil, showing (a) gradient coil contour and (b) magnetic field distribution of ROI of the XoY plane.

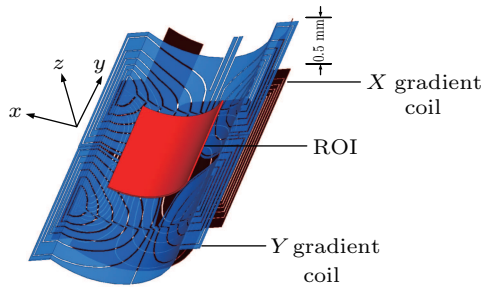


Fig. 7. (color online) Gradient coil structure.

4.2. Experiment results

According to the simulated coil structure, the anti-coil structure design and optimization, and finally using the flexible printed circuit board (PCB) processing, the gradient coil is obtained as shown in Fig. 7.

This study uses the United States FW.Bell8030 Gauss meter, 3D stepper platform, Agilent6653A current source constitutes a measurement platform shown in Fig. 10. When 1 A current is applied, the magnetic field above the gradient coil is measured to obtain the B_x distributions of the X and Y gradient coil in the ROI as shown in Fig. 8. From the measured magnetic field distribution map, it follows that the designed gradient coil basically satisfies design requirements. However, due to uneven wiring and processing errors and other effects, there is a certain deviation from the simulation results.

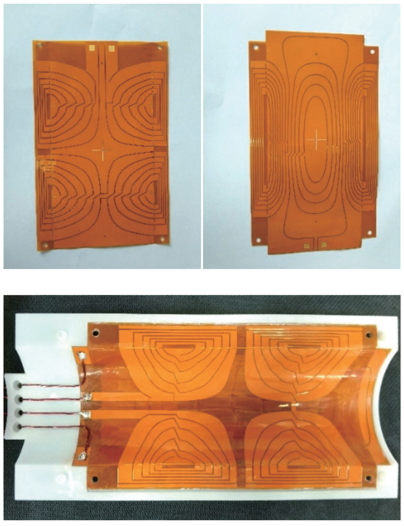


Fig. 8. (color online) Gradient coil physical map.

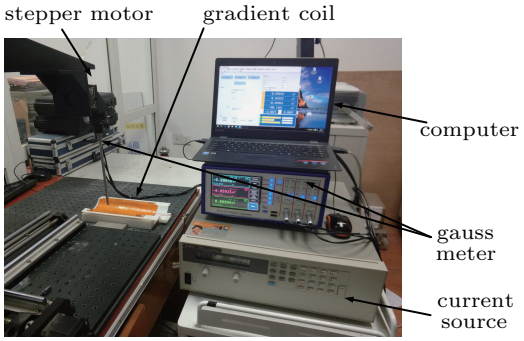


Fig. 9. (color online) Experimental platform of measurement.

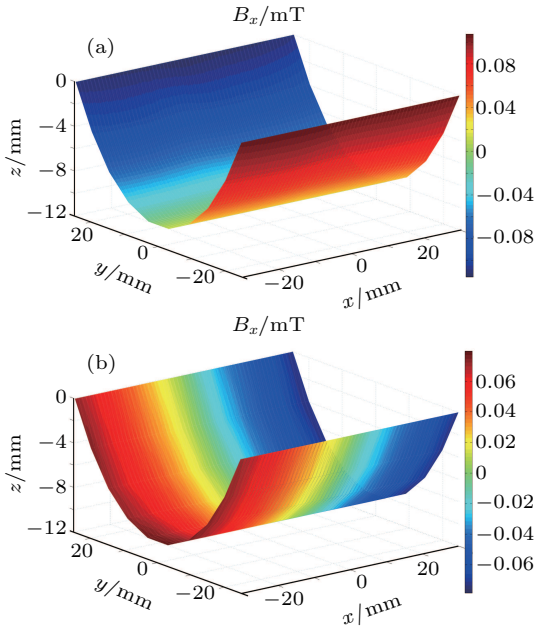


Fig. 10. (color online) Measured magnetic fields of gradient coil ROI, produced by (a) X gradient coil and (b) Y gradient coil.

Then the results measured from X gradient coil and Y gradient coil and simulation results are analyzed and compared in Tables 1 and 2, the results indicate that the measured coil efficiency and linearity are slightly worse than the simulation

results, but meet the design requirements, to achieve the function of the gradient coil.

Table 1. *X* gradient coil parameter alignment.

Item	Efficiency/mT·m^{-1}·A^{-1}	Linearity/%
Simulation	4.54	2.41
Measurement	4.01	2.82

Table 2. *Y* gradient coil parameter alignment.

Item	Efficiency/mT·m^{-1}·A^{-1}	Linearity/%
Simulation	1.46	2.97
Measurement	1.70	3.56

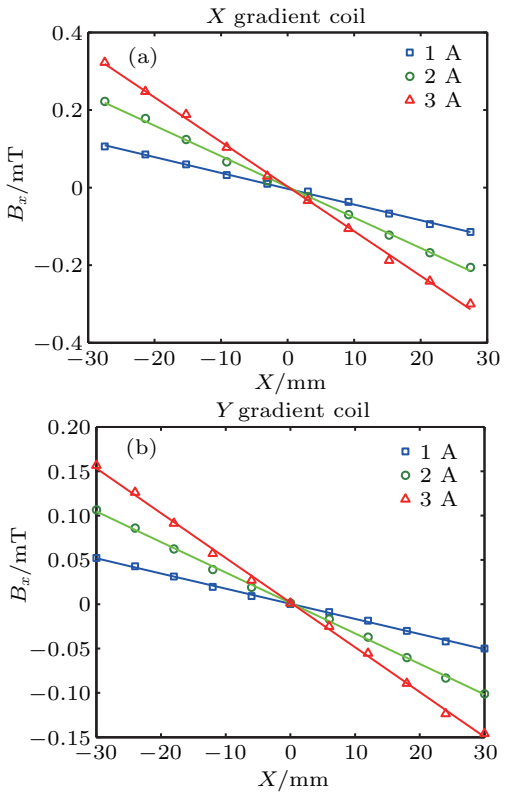


Fig. 11. (color online) Measured central axial magnetic field of ROI, produced (a) *X* gradient coil and (b) *Y* gradient coil.

Table 3. *X* gradient coil.

Current/A	Maximum temperature rise/°C	Efficiency /mT·m^{-1}·A^{-1}	Linearity/%
1	2.2	4.01	2.82
2	8.5	3.89	3.45
3	18.3	3.78	4.21

We inject direct currents (DCs) of 1 A, 2 A, and 3 A into the *X* and *Y* gradient coil, and obtain the distribution of the central axial magnetic field of ROI, which is shown in Fig. 11. According to the data we measured, which are shown in Tables 3 and 4, we find that when the injected current increases, the coil temperature will increase, and the coil efficiency and linearity decline to different degrees, but the variation range is acceptable. Moreover, in the actual MRI work, the alternating current (AC) pulse square wave is applied to the gradient coil, and its calorification is smaller than the DC test result, so the coil performance is better.

Table 4. *Y* gradient coil.

Current/A	Maximum temperature rise/°C	Efficiency /mT·m^{-1}·A^{-1}	Linearity/%
1	1.5	1.70	3.56
2	6.8	1.68	3.78
3	13.2	1.68	4.23

5. Conclusions

First of all, in this work we design a unilateral magnet in the field of medical local imaging of mobile MRI equipment and realize the arc-shaped target magnetic field distribution with a natural gradient in the area of 10 mm cylindrical side arc surface above the magnet.

Then based on the principle of the unilateral specific direction of the main magnetic field, the gradient coil design adopts the equivalent magnetic dipole method. According to the requirements for this unilateral magnet, the gradient coil wiring area and the ROI are designed to be cylindrical side arc surface, in this paper, the design method for the above situation has been improved and optimized.

Finally, we apply the coil design results to real coils, use mature measurement platform to measure the gradient coil, and find that the magnetic field distribution in the ROI is close to the simulation results. However, because of wiring problems such as asymmetry, there are still some deviations.

The mobile UMRI will be widely used, especially for the open imaging of large volume samples (such as localized breast imaging). Gradient coil design for unilateral magnets is an important research foundation for the study of the mobile UMRI, so it needs to be further studied. In the future work, we will further investigate the sequence and imaging results of UMRI in combination with the existing UMRI equipment.

References

[1] Blümich B 1988 *Angew. Chem. Int. Ed.* **27** 195
[2] Callaghan P T 1992 *Z. Phys. Chem.* **176** 132
[3] Xu Z, Meng K K and Cheng J Y 2015 *Int. J. Appl. Elec. & Mech.* **47** 777
[4] Xu Z, Cui X J and Meng K K and Xia YF 2016 *IEEE Sens. J.* **16** 1168
[5] He Z H and He W 2016 *Appl. Magn. Reson.* **47** 1
[6] He Z H, He W, Wu J M and Xu Z 2017 *Sensors* **17** 526
[7] Casanova F and Blümich B 2003 *J. Magn. Reson.* **163** 38
[8] Turner R 1993 *Magn. Reson. Imag* **11** 903
[9] Garrett M W 1951 *J. Appl. Phys.* **22** 1091
[10] Schenck J F, Hussain M A and Edelstein W A (U.S. Patent) 4646024 [1983-11-2]
[11] Brideson M A, Forbes L K and Crozier S 2001 *John Wiley and Sons Ltd.* **14** 9
[12] Turner R 1986 *J. Phys. D: Appl. Phys.* **19** 147
[13] Wang L Q and Wang W M 2014 *Chin. Phys. B* **23** 589
[14] Liu W T, Zu D L and Tang X 2010 *Chin. Phys. B* **19** 018701
[15] Lopez H S, Liu F, Poole M and Crozier S 2009 *IEEE Trans. Magn.* **45** 767
[16] Lopez H S, Poole M and Crozier S 2009 *J. Magn. Reson.* **199** 48
[17] Liu W T, Casanova F and Blumich B 2012 *Appl. Magn. Reson.* **42** 101
[18] Xu Y J, Chen Q Y, Zhang G C, Pei Z and Yang X 2015 *Appl. Magn. Reson.* **46** 823